J Mater Sci (2020) 55:1614–1626

Energy materials

Benzene–toluene–xylene (BTX) from p-cresol by hydrodeoxygenation over nickel phosphide catalysts with different supports

Liuyi Pan[1,2], Yulong He[1], Menglong Niu[3], Yong Dan[1], and Wenhong Li[1,*]

[1] School of Chemical Engineering, Northwest University, Xi'an 710069, Shaanxi, People's Republic of China
[2] College of Chemistry and Chemical Engineering, Baoji University of Arts and Sciences, Baoji 721013, Shaanxi, People's Republic of China
[3] College of Chemistry and Chemical Engineering, Xi'an Shiyou University, Xi'an 710065, Shaanxi Province, People's Republic of China

Received: 8 May 2019
Accepted: 12 September 2019
Published online: 16 October 2019

ABSTRACT

Ni_2P catalysts supported on different supports, such as SiO_2 from different sources, Al_2O_3, TiO_2 and ZrO_2 were prepared for the hydrodeoxygenation of p-cresol (monocyclic phenol model in coal tar). The reaction was carried out on a fixed-bed reactor at a temperature of 330–390 °C under 2 MPa. The order of conversion of p-cresol was as follows: Ni_2P/SiO_2-2 > Ni_2P/SiO_2-3 > Ni_2P/SiO_2-1 > Ni_2P/Al_2O_3 > Ni_2P/ZrO_2 > Ni_2P/TiO_2. Ni_2P/SiO_2-3 shown higher DDO path selectivity, resulting in the conversion of p-cresol of 93% and a selectivity of 72.6% for BTX products under the reaction temperature of 370 °C with LHSV of 0.5 h^{-1}. This catalyst was also used for the hydrodeoxygenation of the crude phenolic mixture extracted from coal tar, which shown that the phenol deoxidation rate was 87.6% and the BTX product selectivity was 73.7% by GC–MS.

Introduction

The low-temperature fraction of low-temperature coal tar is rich in phenolic compounds, especially monocyclic phenols. The crude phenol product obtained by the extraction of coal tar can be further purified to obtain a high-purity phenol product, but at the same time, a large amount of phenol-containing wastewater is also produced [1, 2]. Therefore, the hydrodeoxygenation of phenols in coal tar can not only facilitate the production of downstream BTX products, but also improve the quality of processed light fuels [3].

The research on hydrodeoxygenation technology and related catalysts mainly focuses on the upgrading of bio-oil. The guaiacol selected as an oxygenate model for hydrodeoxygenation studies has been widely reported [4–8]. In the hydrotreating process of

Address correspondence to E-mail: liwenhong@nwu.edu.cn

https://doi.org/10.1007/s10853-019-04037-y

coal tar, in addition to the main removal of S and N heteroatoms, the traditional $CoMoS/Al_2O_3$ is also used to remove oxygen heteroatoms [5]. The widely studied hydrodeoxygenation catalysts mainly include monometallic catalysts with active metals of Ni, Mo, Co [9–11] and noble metals Pt and Pd [12, 13], bimetallic catalysts [14–16] and metal phosphide catalysts including Ni_2P, CoP and MoP [4, 17, 18] etc. In previous studies, the type of support had a significant effect on the reactivity in the catalytic process, the selectivity of the product and the stability or catalyst life. The inexpensive and readily available alumina carrier can provide more acidic centers than neutral supports which facilitates the activation and cracking of C–O bonds during hydrogenation, but it causes severe carbon deposition and is sensitive to a large amount of water generated during hydrodeoxygenation [19]. Therefore, ZrO_2, TiO_2, SiO_2 and MgO [7, 20, 21], as well as zeolite [22–25] such as SBA-15 and ZSM-5, are used for the loading of active metals for hydrodeoxygenation. Complex oxide supports, such as SiO_2–ZrO_2 and Al_2O_3–TiO_2, also have been studied on hydrodeoxygenation catalysts [26].

Phenol hydrodeoxygenation involves two main reaction pathways: The HYD path is first subjected to hydrogenation of aromatic ring and then the C(sp^3)–O bond is cleaved by dehydration to obtain a cycloalkane product, the DDO path is the direct cleavage of the C(sp^2)–O bond to obtain an aromatic product [27]. Due to the different physical structures, acidity and the combination of support and active metal, the catalysts with different supports can strengthen the DDO reaction path to different extent in the process of phenol hydrodeoxygenation, resulting in BTX predominating in the hydrogenation product [6, 28]. Xu and Jiang [6] prepared a series of Ni/Fe catalysts supported on different supports for the hydrodeoxygenation of guaiacol. They found that, under the similar conversion, the BTX selectivity of Fe/Ni/HY zeolite was 14%, while Fe/Ni/HBeta and Fe/Ni/ZSM-5 were only 5.5% and 6%, respectively. Oyama et al. [29] studied that the final product of guaiacol hydrodeoxygenation on Ni_2P/SiO_2 had a large amount of benzene in addition to phenol and cathol, while Ni_2P/ZSM-5 and Ni_2P/FCC mainly get cathol products, which had a great relationship with the acidity of the support. The Ni_2P/hierarchical ZSM-5 prepared by Berenguer et al. [22] was compared with conventional Ni_2P/SiO_2 for the study of hydrodeoxygenation of p-cresol. This catalyst first catalyzed the conversion of almost all p-cresol to 3-methylcyclohexanol and then rapidly deoxidizes to cyclohexane, while Ni_2P/SiO_2 catalyzed only about 60% conversion with a small amount of toluene product.

In this work, a series of Ni_2P catalysts supported on different supports, such as SiO_2-1, SiO_2-2, SiO_2-3, γ-Al_2O_3, ZrO_2 and TiO_2, were prepared to study the selectivity of BTX product in the hydrodeoxygenation product of p-cresol. Under the relatively low reaction pressure (2 MPa) and the reaction temperature range of 330–390 °C, we carried out hydrogenation experiments on a fixed-bed reactor, and compare the reaction performance and product distribution of catalysts with different supports. In addition, we also studied the conversion of BTX products obtained by hydrodeoxygenation of crude phenol obtained by extraction from coal tar.

Experimental

Preparation of catalysts

SiO_2-1 is Type B silica gel purchased from a catalyst plant in Qingdao. SiO_2-2 was prepared from Nankai University. SiO_2-3 was model Q10 purchased from Fuji Silysia (Japan). The γ-Al_2O_3 was prepared by calcination of pseudo-boehmite at 550 °C for 3 h. ZrO_2 and TiO_2 were obtained by precipitating the sulfate and nitrate solutions at a pH of 10, respectively [30, 31].

The supported Ni_2P catalyst was prepared by incipient wetness impregnation method with Ref. [32], and the P/Ni molar ratio was selected to be 1.2 at a loading ratio of 20 wt% by Ni. Five sets of 14.86 g $Ni(NO_3)_2{\cdot}6H_2O$ (≥ 8.0%, Aladdin) and 7.05 g of $NH_4H_2PO_4$ (99%, Aladdin) were respectively weighed and dissolved in a certain amount of deionized water (the amount of water was determined according to the water absorption rate of the carrier) by ultrasound. After drying at 200 °C for 2 h, the carrier was added dropwise to the nickel nitrate solution, and then dried at 200 °C and then calcined at 500 °C for 3 h. The precursor was then impregnated with $NH_4H_2PO_4$ solution and dried at 200 °C.

These catalyst precursors should be subjected to a reduction treatment before being used in the reaction. The reduction conditions, except for the catalyst

supported on γ-Al_2O_3, were as follows: H_2/N_2 (10% H_2) mixed gas with the flow rate of 200 mL/min, while the temperature was raised from 30 to 350 °C at 5 °C/min, maintained for 60 min at 350 °C, and then raised again from 350 to 650 °C at 2 °C/min, and maintained for 4 h. The sample was then passivated in N_2 for 10 h after cooled to room temperature in H_2. Ni_2P/Al_2O_3 was reduced at 700 °C, mainly based on H2-TPD results.

Characterization of catalysts

The nitrogen adsorption–desorption measurement was performed on a Quantachrome SI at − 196 °C after degassed under vacuum at 350 °C for 3 h. The average pore diameter was calculated using the desorption branch of the isotherm according to the BJH method.

X-ray diffraction (XRD) was carried on Bruke D8 Advance with Cu Ka radiation (k = 1.5406 Å) operated at 40 kV and 30 mA. Diffraction intensities were collected within a 2θ range from 10° to 80° at a rate of 10°/min.

H_2 temperature-programmed reduction(H_2-TPR) was measured on a self-built test instrument including an U-tube reactor, heating jacket and a thermal conductivity detector (TCD).The catalyst sample (80 mg) was kept in the reactor, then dried and degassed under N_2 flow (50 mL/min) at 200 °C for 2 h. Reduction was conducted at a heating rate of 10 °C/min from 200 to 950 °C in a 10 vol% H_2/N_2 flow(50 mL/min).

NH_3-TPD patterns were performed on the AutoChem1 II 2920(MICROMERITICS INSTRUMENT CORP). Before TPD studies, catalyst was pre-treated by flowing high-purity H_2 stream at 650 °C for 60 min, cooling to 100 °C. After pretreatment, the catalyst was adsorbed at flowing (20 mL/min) 10% NH_3 and He mixed gas at 40 °C for 2 h and then removed the NH_3 of physical absorption by flowing He. Finally, the sample was heated to 600 °C at a rate of 5 °C/min under a He flow (30 mL/min), desorbed NH_3 was detected with TCD.

X-ray photoelectron spectroscopy (XPS) was measured by using K-Alpha$^+$ (Thermo fisher Scientific) with Al Kα radiation (1486.6 eV).Binding energies were referenced to the C1s at 284.8 eV.

HDO test

The HDO experimental device was a fixed-bed reactor (I.D. 17 mm, length 1200 mm) filled with 30 mL of catalysts which was in our previous study [33].The catalysts were loaded in the middle of the bed with quartz sands of 60–80 meshes. P-cresol (≥ 98.0%, Aladdin) was injected through the feedstock pump and then was mixed with the H_2 before entering the bed. Before the hydrogenation reaction, catalysts were filled in the reactor and reduced at 450 °C for 2 h in a H_2 flow(100 mL/min), then the reactor cooled to reaction temperature in H_2 atmosphere.

Liquid products were analyzed by a GC–MS system (Shimadzu QP2010 Plus) and a GC(Agilent 9790A) equipped with HP-INNOWax polar column (30 m * 0.32 mm * 0.5 mm)and a FID detector. During the experiment, the main hydrogenation products were quantitatively analyzed by external standard method, and products in very little content like biphenyls and olefin were not calculated.

The conversion, selectivity of main reaction product and turnover frequency (TOF) were calculated as follows:

$$\text{Conversion}\,[\%] = \frac{N(p-\text{cresol})\text{in} - N(p-\text{cresol})\text{out}}{N(p-\text{cresol})\text{in}} \times 100$$

$$\text{Selectivity}\,[\%] = \frac{Ni}{N(p-\text{cresol})\text{in} - N(p-\text{cresol})\text{out}} \times 100$$

$$\text{TOF} = \left(\frac{Q \times \rho}{M} \times C\right) \Big/ \left(\frac{m \times L}{M} \times D\right)$$

N, Q, ρ, C, M, m, L and D are the content, volume flow rate, density of feed, conversion, molecular weight, the mass of catalyst, loadings of Ni and dispertion, respectively [34].

Results and discussion

Characterization of the catalysts

Structural characterization

The specific surface area, pore volume and pore size are listed in Table 1, and N_2 adsorption–desorption isotherms and pore size distribution are shown in Fig. 1. The specific surface areas of Ni_2P/SiO_2 were relatively large, but the pore size was quite different, which followed the order: SiO_2-3 (10.11 nm) > SiO_2-1

Table 1 Physical properties of catalysts with different supports

	S_{BET}[a] (m^2/g)	Pore volume[a] (m^3/g)	Pore size[a] (nm)	Particle size[b] (nm)	Dispersion[c] (%)	NH_3 uptake catalyst/support (μmol/g)
Ni_2P/SiO_2-1	281	0.61	6.98	20.6	4.4	230/11
Ni_2P/SiO_2-2	231	0.55	6.22	16.3	5.5	342/17
Ni_2P/SiO_2-3	259	0.62	13.11	25.1	3.6	336/12
Ni_2P/Al_2O_3	188	0.67	6.15	18.7	4.8	419/376
Ni_2P/ZrO_2	109	0.43	5.21	17.6	5.1	168/146
Ni_2P/TiO_2	74	0.32	3.90	31.7	2.8	106/151

[a]BET surface areas determined by N_2 adsorption–desorption

[b]Particle size calculated by Scherrer Formula

[c]The dispersion (D) calculated with particle size (d) by equation $D \approx 0.9/d$

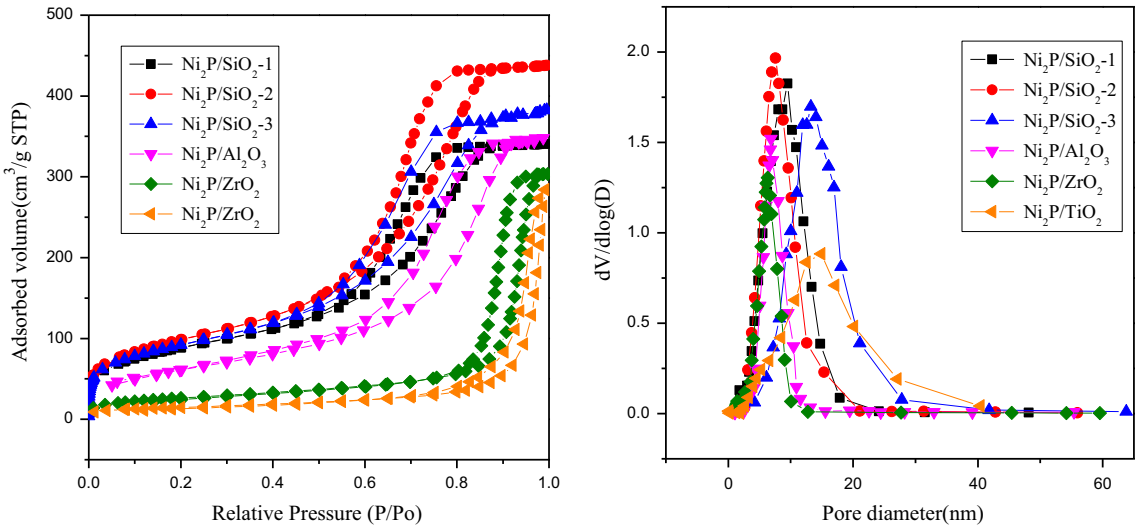

Figure 1 N_2 adsorption–desorption isotherms and pore size distributions for the catalysts with different supports.

(7.48 nm) > SiO_2-2 (6.22 nm). In comparison, the prepared ZrO_2 and TiO_2 supports had poor specific surface area, and the pore volume and pore size were also smaller.

N_2 adsorption–desorption isotherms for each of the catalysts shown a typical type IV, and their pore size distributions were concentrated at 0–50 nm, showing the characteristics of a typical mesoporous material. The curves of the three silica supports had obvious saturated adsorption platforms, which belong to the typical H2 type hysteresis loop, indicating that the pore size distribution was wide and the pore structure was complicated. The isothermal of ZrO_2 and γ-Al_2O_3 was the H1 type hysteresis loop, showing a relatively narrow pore size distribution. The curves of TiO_2 belong to the H3 type hysteresis loop, indicating that the pore size was relatively large and uneven.

XRD characterization

Figure 2 shows the XRD patterns of the freshly prepared Ni_2P samples supported on the different supports. Obvious sharp peaks belonging to the nickel phosphide diffraction peak were observed at 2θ = 40.7° (111), 44.6° (201), 47.4° (210), 54.2° (300), 55.0° (201) (JCPDS 74-1385), which indicated that the Ni_2P active phase was obtained by the reduction. It is not certain that the reduced metallic nickel over these catalysts was absent because the diffraction peak of the metallic nickel observed at 2θ = 44.5° (111) (JCPDS 87-0712) may coincide with Ni_2P [34]. However, from the analysis of the intensity of the

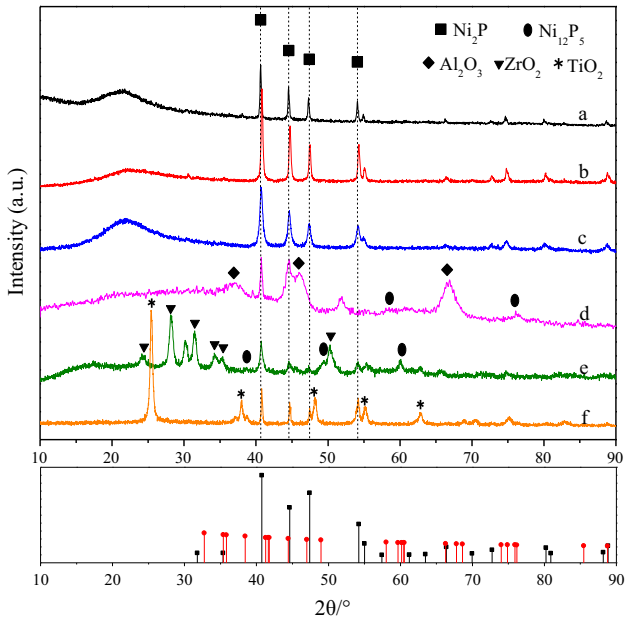

Figure 2 X-ray diffraction patterns of catalyst with different supports. a Ni_2P/SiO_2-1, b Ni_2P/SiO_2-2, c Ni_2P/SiO_2-1, d Ni_2P/Al_2O_3, e Ni_2P/ZrO_2, f Ni_2P/TiO_2.

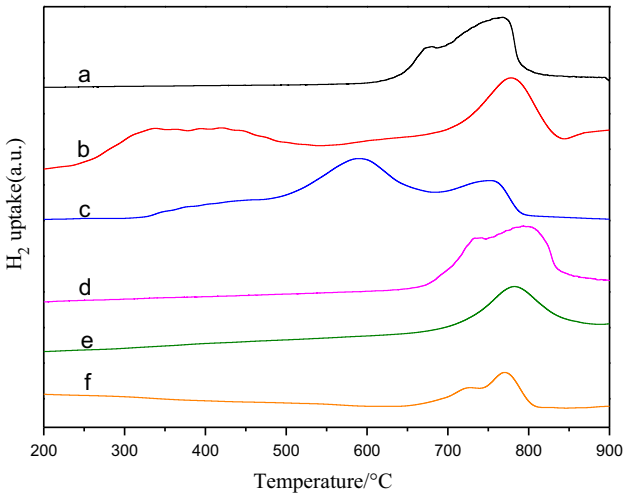

Figure 3 H_2-TPR profiles of catalysts with different supports. a Ni_2P/SiO_2-1, b Ni_2P/SiO_2-2, c Ni_2P/SiO_2-1, d Ni_2P/Al_2O_3, e Ni_2P/ZrO_2, f Ni_2P/TiO_2.

diffraction peak, Ni_2P/SiO_2-2 may contain metallic nickel or nickel oxide. Further, the diffraction peak of $Ni_{12}P_5$ at $2\theta = 38.6°$, 49.4°, 58.5° and 60.1° (JCPDS 74-1381) was observed in the patterns of Ni_2P/Al_2O_3 and Ni_2P/ZrO_2 [35].

The diffraction peak at $2\theta = 40.7°$ was selected for the Scherrer Formula to calculate the partical size of different catalysts, and then the dispersion of the active site was calculated by the relationship between the dispersion D and the partical size [7]. The particle size shown in Table 1 was as follows: Ni_2P/TiO_2 (31.7 nm) > Ni_2P/SiO_2-2 (25.1 nm) > Ni_2P/SiO_2-1 (20.6 nm) > Ni_2P/Al_2O_3 (18.7 nm) > Ni_2P/ZrO_2 (17.6 nm) > Ni_2P/SiO_2-2 (16.3 nm). Therefore, the dispersion degree was as follows: Ni_2P/SiO_2-2 (5.5%) > Ni_2P/ZrO_2 (5.1%) > Ni_2P/Al_2O_3 (4.8%) > Ni_2P/SiO_2-1 (4.4%) > Ni_2P/SiO_2-3 (3.6) > Ni_2P/TiO_2 (2.8%).

H_2-TPR characterization

Figure 3 shows the H_2-TPR spectra of catalysts with different supports dried at 200 °C. The peak below 700 °C was attributed to the reduction of the nickel species, while the peak above 700 °C was attributed to the reduction peak of the P–O bond [4, 36]. For the three silica supports, the reduction temperature of the P–O bond was 766 °C (Ni_2P/SiO_2-1), 777 °C (Ni_2P/SiO_2-2) and 751 °C (Ni_2P/SiO_2-3), respectively, showing that Ni and P had a stronger interaction in the oxidized precursor on the SiO_2-2 support. Compared with the pattern of Ni_2P/SiO_2-1, the reduction peak of nickel oxide in the pattern of Ni_2P/SiO_2-3 first appeared at about 400 °C. The reduced Ni promoted the formation of highly active H_2 species, thereby promoting the reduction of P–O, which ultimately leaded to a lower P–O bond reduction peak temperature [17, 20, 37]. In the profiles of Ni_2P/Al_2O_3 and Ni_2P/ZrO_2,the reduction temperature of the P–O bond were 797 °C and 784 °C, respectively, which were higher than that of the silica support, meaning a strong interaction between the phosphate precursor and the support [34]. This strong interaction prevented the precursor $Ni_{12}P_5$ from being completely reduced to a pure Ni_2P phase, which can be reflected from the XRD pattern [38]. In addition, comparing the hydrogen consumption peak intensity of each catalyst, Ni_2P/TiO_2 and Ni_2P/ZrO_2 showed a small hydrogen consumption, which may mean that the number of Ni_2P active phases formed was small.

NH_3-TPD Characterization

Figure 4 shows the NH_3-TPD profiles of catalysts with Ni_2P supported on the SiO_2-1, SiO_2-2, SiO_2-3, Al_2O_3, TiO_2 and ZrO_2. The NH_3 adsorption amount of each support and catalyst is listed in Table 1. The

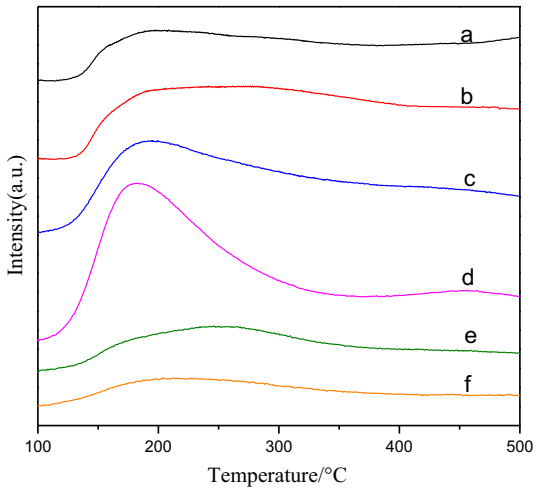

Figure 4 NH_3-TPD profiles of catalysts with different supports. a Ni_2P/SiO_2-1, b Ni_2P/SiO_2-2, c Ni_2P/SiO_2-1, d Ni_2P/Al_2O_3, e Ni_2P/ZrO_2, f Ni_2P/TiO_2.

silica support generally considered to be non-acidic was detected to have almost no adsorption to NH_3 before loading. However, after loading the Ni_2P active phase, it was observed that a obvious peak centered at 150–200 °C was attributed to the weak acid sites and a wide shoulder peak shown at 300–350 °C was attributed to a medium acid sites. Oyama et al. [29] and Abu and Smith[39] concluded that the Ni_2P catalyst had both Brønsted and Lewis acids. Brønsted acid sites were attributed to unreduced phosphorus species, mainly from PO–H groups, while Lewis acids were derived from the electron transfer of Ni in Ni_2P. The order of adsorption of ammonia on the catalyst supported on three silica supports is: SiO_2-2 > SiO_2-3 > SiO_2-1. The stronger acidity of Ni_2P/SiO_2-2 may be due to unreduced nickel oxide and nickel silicate species, which corresponded to the TPR results. The γ-Al_2O_3 was much more acidic than the silica support, mainly because Al^{3+} can provide more acid sites [38]. However, after loading, the acidity of Ni_2P/Al_2O_3 was only slightly enhanced compared to the unsupported carrier, indicating that Ni_2P can supplement a certain amount of acid sites, but it also covered the original acid site of the carrier itself [29, 40]. The acidity of the zirconia support was weaker than that of γ-Al_2O_3, but the change in acidity after loading was similar. The acidity of the TiO_2 support after loading was obviously decreased, which may be due to the relatively small amount of Ni_2P formed by the reduction process resulting in the accumulation of phosphate on the surface.

XPS characterization

The surface distribution, oxidation state and integration of Ni and P are measured by XPS shown in Fig. 5. The XPS binding energy and distribution are listed in Table 2. The Ni $2p_{3/2}$ spectrum can be observed three contributions [32, 34, 41]. The first one was located at 853 eV, which was attributed to the $Ni^{\delta+}$ formed by the electron transfer from Ni to P in Ni_2P and also confirmed the formation of active phase Ni_2P. The second and third were located at 856.5 eV and 862 eV attributed to Ni^{+} ion and shakeup satellite, respectively. Comparing the P spectra of the catalysts with different supports, although the peaks were slightly different, there were mainly three contributions observed [32, 34, 41]. One is a peak at 129.6–129.9 eV, which is attributed to $P^{\delta-}$ covalently bound to $Ni^{\delta+}$ in the active phase Ni_2P. The second is the unreduced $(HPO_3H)^-$ anion at 133.5 eV. The third is attributed to the phosphate species P^{5+} at 134.5 eV, possibly due to passivation or oxidation.

In spectra for Ni 2*p*, the peak intensity of the silica support at 853 eV was large, indicating that the neutral silica carrier favored the reduction of nickel oxide and phosphorus oxide to form the active phase Ni_2P. However, the peak intensity on SiO_2-2 was relatively small compared to the other two, probably because of the strong interaction between the precursors of Ni and P on the support, as can be seen from the TPR, which hindered the formation of active phase Ni_2P. Comparing the P 2*p* spectra, the peak at 129 eV was not detected on the alumina and zirconia supports, but the formation of the Ni_2P active phase in the bulk phase can be observed from the XRD results. It may be that the acidic carrier readily combined with excess phosphorus to form a phosphate form, such as $AlPO_4$ [37, 42, 43], which can be confirmed from the XPS results that the proportion of PO^{4-} species was higher than others. The carrier competed with Ni for the P species, resulting in the resistance of the formation of Ni_2P or other phase Ni_xP_y. In addition, it was also possible that the acidity of the support enhanced the surface oxidation phenomenon, causing the reduced Ni_2P to be oxidized to phosphorus oxides [18, 34, 44]

The Ni/P molar ratio of each catalyst is lower than the theoretical load of 0.83. Some authors [18]

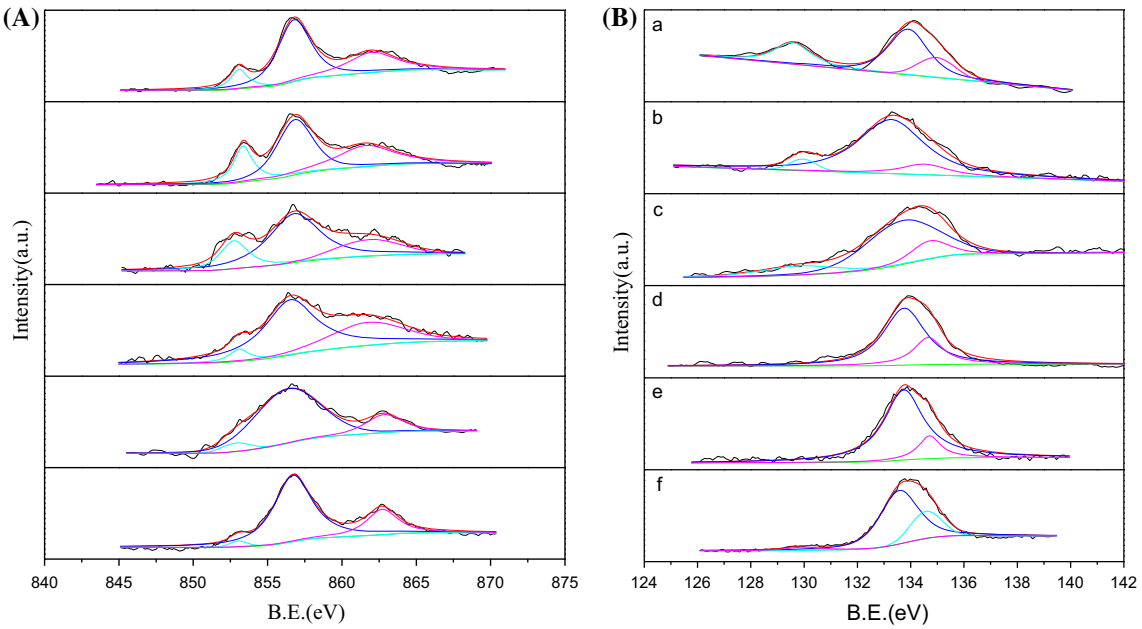

Figure 5 XPS spectra for catalysts with different supports **A** Ni 2*p* core level spectra and **B** P 2*p* core level spectra. a Ni_2P/SiO_2-1, b Ni_2P/SiO_2-2, c Ni_2P/SiO_2-1, d Ni_2P/Al_2O_3, e Ni_2P/ZrO_2, f Ni_2P/TiO_2.

Table 2 The XPS spectra in the Ni 2*p* and P 2*p* regions for Ni_2P with different supports

	Ni			P			Ni/P
	Ni_2P	Ni^{2+}	Sat.	Ni_2P	HPO_3H^-	PO_4^{3-}	
Ni_2P/SiO_2-1	853.1 (11.1)	856.8 (58.6)	861.9 (30.3)	129.6 (25.5)	133.8 (56.3)	134.6 (18.2)	0.38
Ni_2P/SiO_2-2	853.3 (19.8)	856.8 (47.7)	861.6 (32.5)	129.9 (5.3)	133.3 (83.2)	134.5 (11.5)	0.31
Ni_2P/SiO_2-3	852.7 (19.3)	856.8 (61.5)	861.8 (19.2)	129.9 (16.3)	133.7 (67.5)	134.6 (16.1)	0.35
Ni_2P/Al_2O_3	853.1 (5.5)	856.5 (64.4)	861.7 (30.2)	–	133.7 (73.5)	134.7 (26.5)	0.51
Ni_2P/ZrO_2	852.9 (5.1)	856.3 (78.2)	862.0 (16.8)	–	133.7 (84.7)	134.7 (15.3)	0.29
Ni_2P/TiO_2	853.0 (2.6)	856.7 (74.0)	862.7 (23.4)	129.9 (4.4)	133.5 (72.0)	134.6 (23.6)	0.18

concluded that part of P was lost in the form of PH_3 during high temperature reduction. The Ni/P of the silica support was slightly lower than the alumina support, indicating that the loss of phosphorus may be related to the strength of the interaction between the support and phosphorus.

HDC tests

HDO performance of Ni_2P supported on different supports

HDO of p-cresol was tested over the Ni_2P supported on different supports at 370 °C under 2 MPa, and the product distribution results are shown in the Table 3. Through the DDO and HYD reaction paths, the main hydrodeoxygenation products of p-cresol were the aromatic product—toluene and the aromatic saturated product—methylcyclohexane [42, 45]. Benzene and cyclohexane formed by the dealkylation reaction were also detected. In addition, the transalkylation reaction products—phenol and xylene—were also found, which were neglected due to their small content. The order of p-cresol conversion is: Ni_2P/SiO_2-2 > Ni_2P/SiO_2-3 > Ni_2P/SiO_2-1 > Ni_2P/Al_2O_3 > Ni_2P/ZrO_2 > Ni_2P/TiO_2. The Ni_2P catalysts with three silica supports had a higher conversion for p-cresol, probably because they had larger specific surface area and pore size, and were all detected to form pure Ni_2P phase. Moreover, the formed acid center will had synergistic hydrogenation with the Ni_2P active center, so Ni_2P/SiO_2-2 with a higher ammonia adsorption had a stronger hydrogenation activity among the three

Table 3 Effects of different catalysts on the products distribution from HDO (370 °C)

	Ni_2P/SiO_2-1	Ni_2P/SiO_2-2	Ni_2P/SiO_2-3	Ni_2P/Al_2O_3	Ni_2P/ZrO_2	Ni_2P/TiO_2
Conversion	91.9	94.6	93.0	88.5	83.7	77.7
Product distribution						
Cyclohexane	1.0	2.7	0.5	3.7	2.5	0.6
Benzene	0.3	2.3	1.4	2.6	1.4	1.2
Methylcyclohexane	38.1	38.7	21.5	35.4	44.6	21.2
Toluene	49.7	43.2	66.1	27.2	30.9	49.3
p-cresol	8.1	5.4	7.0	7.9	16.3	22.3
S_{BTX}	54.4	48.1	72.6	32.4	38.6	65.0

catalysts with silica supports [25, 46]. Although the Ni_2P/γ-Al_2O_3 also had a good surface state, the transformation of $Ni_{12}P_5$ to Ni_2P phase was hindered due to the strong interaction between the alumina and the phosphorus precursor. Studies had shown that the hydrogenation activity of $Ni_{12}P_5$ was lower than that of the Ni_2P phase, thus causing the reactivity of Ni_2P/γ-Al_2O_3 to be lower than that of the Ni_2P/SiO_2 [32, 42, 43]. The conversion of p-cresol on ZrO_2 and TiO_2 supported Ni_2P catalysts was lower, probably because the specific surface area and pore size were relatively small, which was detrimental to the diffusion of the reactants and the contact of the reactants with the active center.

The selectivity of the BTX product is as follows: Ni_2P/SiO_2-3 > Ni_2P/TiO_2 > Ni_2P/SiO_2-1 > Ni_2P/SiO_2-2 > Ni_2P/ZrO_2 > Ni_2P/Al_2O_3. Oyama and Lee [47] and Seo et al. [48] concluded that the active phase Ni_2P exhibited two crystal structures: The Ni(1) site was quasi tetrahedral surrounded by four nearest-neighbor P atoms, and Ni(2) site was square pyramidal surrounded by five nearest-neighbor P atoms. It indicated that the smaller particle size of Ni_2P depended on the larger number of Ni(2) sites; conversely, the larger particle size of Ni_2P depended on the larger number of Ni(1) sites. Moreover, the study also found that the Ni(1) site was prone to $C_{aromatic}$–S bond cleavage, while the Ni(2) site was prone to hydrogenation saturation of aromatic ring in HDS of 4,6-dimethyldibenzothiophene.

Wu et al. [7] also obtained the similar rule in the study of hydrodeoxygenation of guaiacol in Ni_2P catalysts supported on different supports. Since Ni_2P/SiO_2 had smaller grain size than Ni_2P/ZrO_2 and Ni_2P/Al_2O_3, the DDO and DMO reaction paths dominated during the hydrodeoxygenation process of guaiacol. Comparing the particle size of the Ni_2P catalyst on each support in Table 1, the order of the number of Ni(2) active sites is Ni_2P/TiO_2 > Ni_2P/SiO_2-2 > Ni_2P/SiO_2-1 > Ni_2P/Al_2O_3 > Ni_2P/ZrO_2 > Ni_2P/SiO_2-2. Therefore, under the catalysis of Ni_2P/TiO_2 and Ni_2P/SiO_2-3, the tendency of C–O bond cleavage during the hydrogenation of p-cresol was enhanced, and the selectivity of DDO reaction path is increased, resulting in high selectivity of BTX products in the products. Ni_2P/SiO_2-2 with a smaller grain size had a larger number of Ni(1) sites, and it was also detected to have the active center of metallic nickel (XRD and TPR results), which together promote the HYD path, resulting in a saturated product predominating. Although the conversion of Ni_2P/Al_2O_3 was high, the content of toluene and methylcyclohexane in the product is less, which may be due to the strong acidity of the carrier to produce by-products such as phenol, benzylbenzene and the like.

The fresh Ni_2P catalyst supported on six different supports was used to carry out the hydrodeoxygenation of p-cresol at a reaction temperature of 330–390 °C, a reaction pressure of 2 MPa, an LHSV of 0.5 h^{-1} and a hydrogen-to-oil ratio of 600:1. The conversion and TOF are calculated and presented in Fig. 6. As the temperature increasing, the conversion rate on each catalyst increased, and the highest reaction conversion rate was exhibited at 390 °C. Compared with Ni_2P/SiO_2-3, TOF value calculated by the distribution of nickel over Ni_2P/SiO_2-2 was lower at each temperature, probably because of the active center of metallic nickel whose intrinsic hydrogenation activity was weaker than that of Ni_2P. However, its conversion of p-cresol over Ni_2P/SiO_2-2 was higher, indicating that the dispersion of the active center had a significant effect on the specific activity [34]. The same performance also occurs

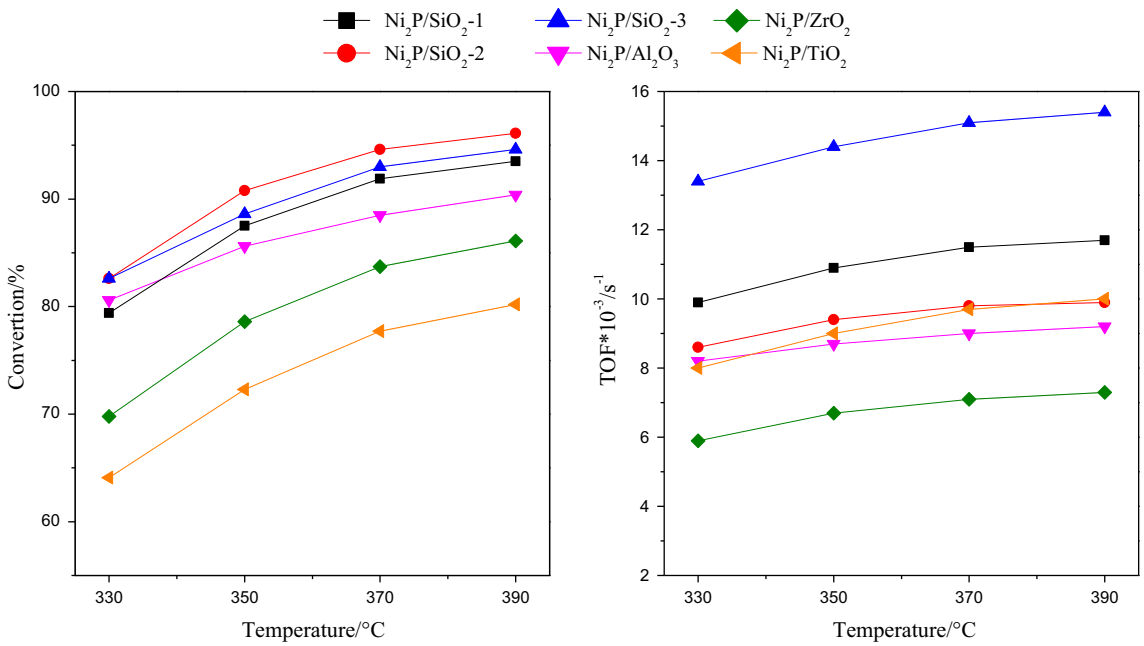

Figure 6 Conversion and TOF on catalysts with different supports (pressure = 2 MPa, LHSV = 0.5 h^{-1}).

between TiO_2 and ZrO_2: ZrO_2 has a lower TOF but a higher reaction conversion effect.

The selectivity of the main products about toluene and methylcyclohexane is shown in Fig. 7. As the reaction temperature increased from 330 to 390 °C, the conversion of toluene almost increased slightly. However, the conversion of methylcyclohexane on catalysts supported on SiO_2-1 and ZrO_2 increased, but in particular, the conversion on Ni_2P/SiO_2-2 with the reaction temperature above 350 °C and Ni_2P/Al_2O_3 with the reaction temperature above 370 °C had a great decrease from 39.8 to 36.6% and 35.4% and 33.1%, respectively, which may be mainly due to the fact that the more acidic catalyst promoted the side reactions such as dealkylation at high temperatures. The selectivity of toluene over Ni_2P on SiO_2-2, SiO_2-2, SiO_2-2, Al_2O_3, ZrO_2 and TiO_2 increased from 50.6 to 55.1%, 45.2 to 46.4%, 66.6 to 71.8%, 27.0 to 28.3%, 32.5 to 38.1% and 61.1 to 64.7%,respectively. In contrast, the selectivity of methylcyclohexane decreased with increasing temperature. DDO and HYD are simultaneously competitive mechanisms, so the distribution of the reaction product has a great influence on the reaction temperature as well as the catalyst. In fact, the result of theoretical calculations is that the bond strength of $C_{aromatic}$–H bond is 84 kJ/mol higher than that of the $C_{aliphatic}$–OH [46]. Although the high reaction temperature allowed both DDO and HYD paths to be enhanced at the same time, it is more favorable to the selectivity of the DDO reaction path. Thus, as the temperature increased, the conversion of cyclohexane increased first, possibly due to a obvious increase in the conversion of the reactants. However, the selectivity of cyclohexane continued to decrease, indicating that the high reaction temperature enhanced the competitiveness of the DDO pathway.

Performance of hydrodeoxygenation on crude phenol extracted from coal tar

The components of the crude phenol mixture extracted from coal tar are mainly phenol and 2-,4-methylphenol, as well as a small amount of dimethylphenol and ethylphenol and very tiny amount of trimethylphenol. The specific composition was analyzed by GC–MS, and the results are shown in Table 4.

Hydrogenation experiments were carried out with Ni_2P/SiO_2-3 under 370 °C, and gas and liquid reaction products were collected after 6 h. The feedstock oil was hydrogenated to obtain about 62 mL oily organic product and about 8 mL water. The amount of gaseous product was less than 2% with very little methane and ethane, mainly due to the fact that the

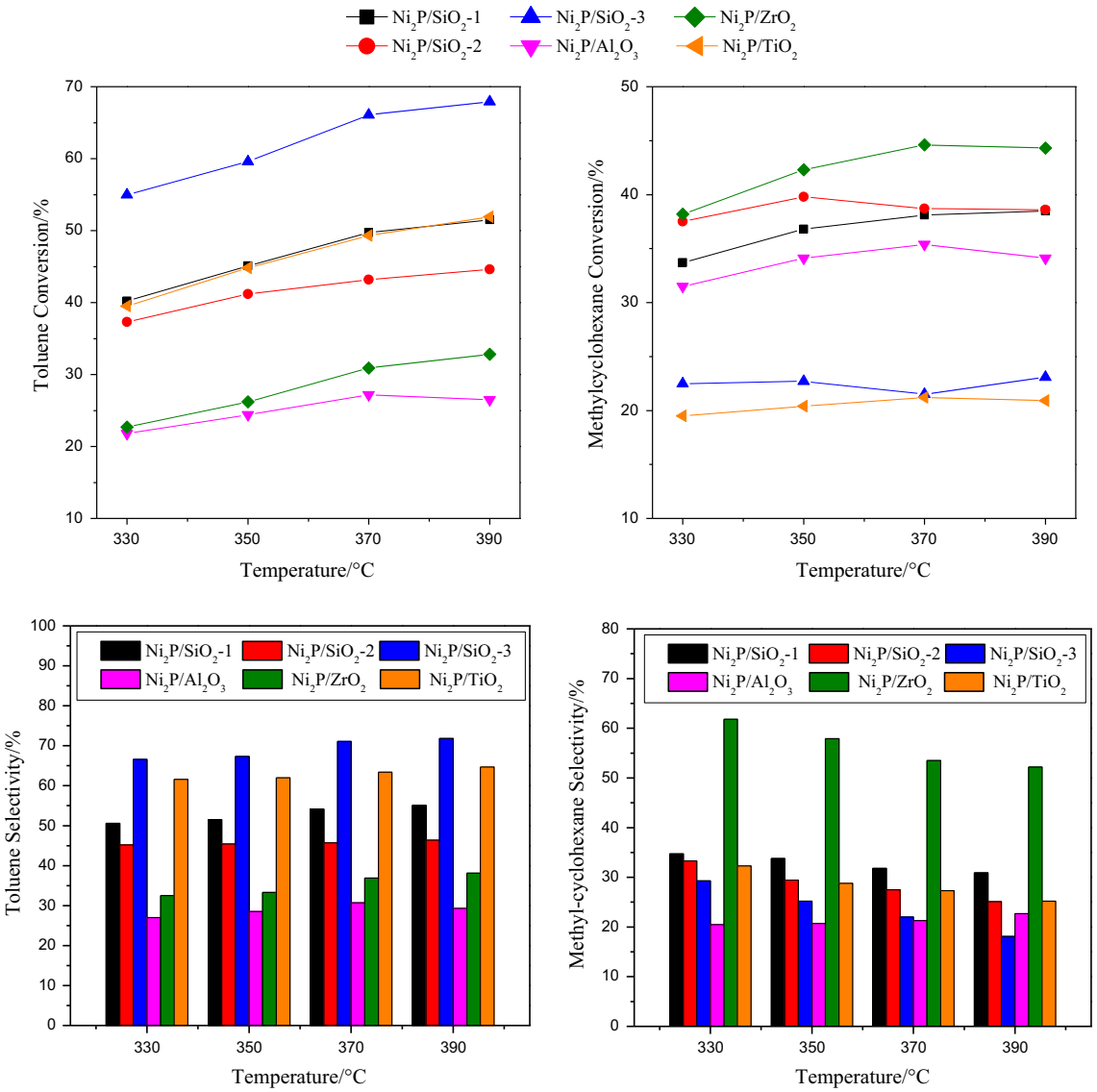

Figure 7 Selectivity of main products toluene and methylcyclohexane on catalysts with different supports.

acidity of this catalyst was very weak. As seen from Table 5, after the hydrogenation reaction, the phenol content and oxygen content of the raw materials were decreased from 98.8 to 12.4% and 12.9 to 1.48%, respectively, indicating that the catalyst had an obvious effect of oxygen removal. Comparing the content of phenol, benzene and cyclohexane before and after the reaction, it indicated that dealkylation and alkylation reactions occur in addition to the removal of oxygen atoms in the hydrogenation process. The total selectivity of the BTX product was 77.3%, confirming that the catalyst also had high selectivity of BTX product for real phenol-containing oils.

Concluding remarks

In this paper, we investigated the effect of five different supports on the selectivity of the hydrodeoxygenation pathway for p-cresol over supported nickel phosphide catalyst. Each catalyst formed a Ni_2P active phase through the reduction process, but the Al_2O_3 and ZrO_2 catalysts also had a $Ni_{12}P_5$ phase which was not completely converted. Compared with SiO_2-2, SiO_2-3 and SiO_2-1 performed higher intrinsic activity at a reaction temperature of 370 °C with LHSV of 0.5 h^{-1}, but SiO_2-2 was detected to have a smaller grain size and a higher degree of active phase dispersion, resulting in a higher specific

Table 4 Main components of crude phenol and products of hydrodeoxygenation determined by GC–MS

	Feed	Product
Phenol	17.75	3.21
o-cresol	17.39	2.17
p-cresol	35.41	4.00
2,6-Xylenol	3.32	0.75
o-Ethylphenol	3.94	0.53
3,4-Xylenol	8.84	0.76
2,3-Xylenol	7.68	0.66
p-Ethylphenol	1.93	0.11
2,5-Xylenol	1.63	0.20
Trimethylphenol	0.87	
Cyclohexane		5.58
Benzene		14.81
Methylcyclohexane		11.36
Toluene		34.34
Ethylcyclohexane		1.62
Ethylbenzene		4.12
Xylene		10.83
Dimethylcyclohexane		4.11
Trimethylbenzene		0.44

Table 5 Properties of materials before and after hydrogenation

	Raw material	Product
The amount of material (mL)	60	67.6
Oxygen content (%)	12.9	1.48
Phenol content (%)	98.8	12.4
Phenol conversion (%)	87.6	
Selectivity of BTX (%)	73.7	

activity. The active phase of nickel phosphide in Al_2O_3 and ZrO_2 contained $Ni_{12}P_5$ which shown lower hydrodeoxygenation activity in addition to Ni_2P, resulting in a lower conversion of p-cresol than that of silica support. The hydrodeoxygenation process followed the competitive DDO and HYD reaction pathways, and the corresponding products were toluene and methylcyclohexane, respectively. The selectivity of toluene in the products of SiO_2-2 and TiO_2 catalysts was higher, probably because the formed Ni_2P was mainly in Ni(1) form with larger particle size, which was beneficial to the DDO reaction path. The SiO_2-2 catalyst used for hydrodeoxygenation of crude phenol mixture extracted by coal tar obtained a high yield of BTX product.

Acknowledgements

We gratefully acknowledge the financial support of the Key Research and Development Program of Shaanxi (2018ZDXM-GY-161 and 2018GY-087).

References

[1] Meng H, Ge C-T, Ren N-N, Ma W-Y, Lu Y-Z, Li C-X (2013) Complex extraction of phenol and cresol from model coal tar with polyols, ethanol amines, and ionic liquids thereof. Ind Eng Chem Res 53:355–362

[2] Zhu L, Deng Y, Chen J, Zhang J (2011) Adsorption of phenol from water by N-butylimidazolium functionalized strongly basic anion exchange resin. J Colloid Interface Sci 364:462–468

[3] Niu M, Sun X, Gao R, Li D, Cui W, Li W (2016) Effect of dephenolization on low-temperature coal tar hydrogenation to produce fuel oil. Energy Fuels 30:10215–10221

[4] Zhao HY, Li D, Bui P, Oyama ST (2011) Hydrodeoxygenation of guaiacol as model compound for pyrolysis oil on transition metal phosphide hydroprocessing catalysts. Appl Catal A Gen 391:305–310

[5] Bui VN, Laurenti D, Afanasiev P, Geantet C (2011) Hydrodeoxygenation of guaiacol with CoMo catalysts. Part I: promoting effect of cobalt on HDO selectivity and activity. Appl Catal B Environ 101:239–245

[6] Xu X, Jiang E (2017) "BTX" from guaiacol HDO under atmospheric pressure: effect of support and carbon deposition. Energy Fuels 31:2855–2864

[7] Wu S-K, Lai P-C, Lin Y-C, Wan H-P, Lee H-T, Chang Y-H (2013) Atmospheric hydrodeoxygenation of guaiacol over alumina-, zirconia-, and silica-supported nickel phosphide catalysts. ACS Sustain Chem Eng 1:349–358

[8] Moon J-S, Kim E-G, Lee Y-K (2014) Active sites of Ni_2P/SiO_2 catalyst for hydrodeoxygenation of guaiacol: a joint XAFS and DFT study. J Catal 311:144–152

[9] Zhang X, Long J, Kong W, Zhang Q, Chen L, Wang T, Ma L, Li Y (2014) Catalytic upgrading of bio-oil over Ni-based catalysts supported on mixed oxides. Energy Fuels 28:2562–2570

[10] Teles CA, Rabelo-Neto RC, de Lima JR, Mattos LV, Resasco DE, Noronha FB (2016) The effect of metal type on hydrodeoxygenation of phenol over silica supported catalysts. Catal Lett 146:1848–1857

[11] Ansaloni S, Russo N, Pirone R (2017) Hydrodeoxygenation of guaiacol over molybdenum-based catalysts: the effect of support and the nature of the active site. Can J Chem Eng 95:1730–1744

[12] Anaya F, Zhang L, Tan Q, Resasco DE (2015) Tuning the acid–metal balance in Pd/ and Pt/zeolite catalysts for the hydroalkylation of m-cresol. J Catal 328:173–185

[13] de Souza PM, Rabelo-Neto RC, Borges LEP, Jacobs G, Davis BH, Sooknoi T, Resasco DE, Noronha FB (2015) Role of Keto intermediates in the hydrodeoxygenation of phenol over Pd on oxophilic supports. ACS Catal 5:1318–1329

[14] Nie L, de Souza PM, Noronha FB, An W, Sooknoi T, Resasco DE (2014) Selective conversion of m-cresol to toluene over bimetallic Ni–Fe catalysts. J Mol Catal A: Chem 388–389:47–55

[15] Yang F, Liu D, Wang H, Liu X, Han J, Ge Q, Zhu X (2017) Geometric and electronic effects of bimetallic Ni–Re catalysts for selective deoxygenation of m-cresol to toluene. J Catal 349:84–97

[16] Sitthisa S, An W, Resasco DE (2011) Selective conversion of furfural to methylfuran over silica-supported NiFe bimetallic catalysts. J Catal 284:90–101

[17] Li K, Wang R, Chen J (2011) Hydrodeoxygenation of anisole over silica-supported Ni_2P, MoP, and NiMoP catalysts. Energy Fuels 25:854–863

[18] Cecilia JA, Infantes-Molina A, Rodríguez-Castellón E, Jiménez-López A (2009) Dibenzothiophene hydrodesulfurization over cobalt phosphide catalysts prepared through a new synthetic approach: effect of the support. Appl Catal B Environ 92:100–113

[19] Laurent E, Delmon B (1994) Influence of water in the deactivation of a sulfided NiMoγ-Al_2O_3 catalyst during hydrodeoxygenation. J Catal 146:281–291

[20] Popov A, Kondratieva E, Goupil JM, Mariey L, Bazin P, Gilson J-P, Travert A, Maugé F (2010) Bio-oils hydrodeoxygenation: adsorption of phenolic molecules on oxidic catalyst supports. J Phys Chem C 114:15661–15670

[21] Yang Y, Gilbert A, Xu C (2009) Hydrodeoxygenation of bio-crude in supercritical hexane with sulfided CoMo and CoMoP catalysts supported on MgO: a model compound study using phenol. Appl Catal A Gen 360:242–249

[22] Berenguer A, Bennett JA, Hunns J, Moreno I, Coronado JM, Lee AF, Pizarro P, Wilson K, Serrano DP (2018) Catalytic hydrodeoxygenation of m-cresol over Ni_2P/hierarchical ZSM-5. Catal Today 304:72–79

[23] Tyrone Ghampson I, Sepúlveda C, Garcia R, García Fierro JL, Escalona N, DeSisto WJ (2012) Comparison of alumina- and SBA-15-supported molybdenum nitride catalysts for hydrodeoxygenation of guaiacol. Appl Catal A Gen 435–436:51–60

[24] Xu X, Jiang E, Li Z, Sun Z (2018) BTX from anisole by hydrodeoxygenation and transalkylation at ambient pressure with zeolite catalysts. Fuel 221:440–446

[25] Sankaranarayanan TM, Berenguer A, Ochoa-Hernández C, Moreno I, Jana P, Coronado JM, Serrano DP, Pizarro P (2015) Hydrodeoxygenation of anisole as bio-oil model compound over supported Ni and Co catalysts: effect of metal and support properties. Catal Today 243:163–172

[26] Zhang X, Long J, Kong W, Zhang Q, Chen L, Wang T, Ma L, Li Y (2014) Catalytic upgrading of bio-oil over Ni-Based catalysts supported on mixed oxides. Energy Fuel 28:2562–2570

[27] Romero Y, Richard F, Brunet S (2010) Hydrodeoxygenation of 2-ethylphenol as a model compound of bio-crude over sulfided Mo-based catalysts: promoting effect and reaction mechanism. Appl Catal B Environ 98:213–223

[28] Mortensen P, Grunwaldt J-D, Jensen P, Jensen A (2013) Screening of catalysts for hydrodeoxygenation of phenol as a model compound for bio-oil. ACS Catal 3:1774–1785

[29] Oyama ST, Onkawa T, Takagaki A, Kikuchi R, Hosokai S, Suzuki Y, Bando KK (2015) Production of phenol and cresol from guaiacol on nickel phosphide catalysts supported on acidic supports. Top Catal 58:201–210

[30] Watanabe S, Ma X, Song C (2009) Characterization of structural and surface properties of nanocrystalline TiO_2–CeO_2 mixed oxides by XRD, XPS, TPR, and TPD. J Phys Chem 113:14249–14257

[31] Takahashi N, Suda A, Hachisuka I, Sugiura M, Sobukawa H, Shinjoh H (2007) Sulfur durability of NO_x storage and reduction catalyst with supports of TiO_2, ZrO_2 and ZrO_2–TiO_2 mixed oxides. Appl Catal B Environ 72:187–195

[32] Sawhill S (2003) Thiophene hydrodesulfurization over supported nickel phosphide catalysts. J Catal 215:208–219

[33] Cui W, Zheng H, Niu M, Zhang S, Li D, Qiao J, Li W (2016) Product compositions from catalytic hydroprocessing of low temperature coal tar distillate over three commercial catalysts. React Kinet Mech Catal 119:491–509

[34] Peyrovi MH, Rostamikia T, Parsafard N (2018) Competitive hydrogenation of benzene in reformate gasoline over Ni supported on SiO_2, SiO_2–Al_2O_3, and Al_2O_3 catalysts: influence of support nature. Energy Fuels 32:11432–11439

[35] Cecilia JA, Infantes-Molina A, Rodríguez-Castellón E, Jiménez-López A (2009) The influence of the support on the formation of Ni_2P based catalysts by a new synthetic approach. Study of the catalytic activity in the hydrodesulfurization of dibenzothiophene. J Phys Chem C 113:17032–17044

[36] Yang Y, Chen J, Shi H (2013) Deoxygenation of methyl laurate as a model compound to hydrocarbons on Ni_2P/SiO_2, Ni_2P/MCM-41, and Ni_2P/SBA-15 catalysts with different dispersions. Energy Fuel 27:3400–3409

[37] Rodriguez JA, Hanson JC, Frenkel AI, Kim JY, Pérez M (2002) Experimental and theoretical studies on the reaction

of H(2) with NiO: role of O vacancies and mechanism for oxide reduction. J Am Chem Soc 124:346–354

[38] Van Veen JAR, Hendriks PAJM, Andrea RR (1990) Chemistry of phosphomolybdate adsorption on alumina surfaces. 2. The molybdate/phosphated alumina and phosphomolybdate/alumina systems. J Phys Chem 94:5282–5285

[39] Abu II, Smith KJ (2007) HDN and HDS of model compounds and light gas oil derived from Athabasca bitumen using supported metal phosphide catalysts. Appl Catal A Gen 328:58–67

[40] Kim Y-S, Lee G-N, Yun Y-K (2014) Novel Ni_2P/zeolite catalysts for naphthalene hydrocracking to BTX. Catal Commun 45:133–138

[41] Zarchin R, Rabaev M, Vidruk-Nehemya R, Landau MV, Herskowitz M (2015) Hydroprocessing of soybean oil on nickel-phosphide supported catalysts. Fuel 139:684–691

[42] Sawhill S, Layman K, Vanwyk D, Engelhard M, Wang C, Bussell M (2005) Thiophene hydrodesulfurization over nickel phosphide catalysts: effect of the precursor composition and support. J Catal 231:300–313

[43] Decanio EC, Edwards JC, Scalzo TR, Storm DA, Bruno JW (1991) FT-IR and solid-state NMR investigation of phosphorus promoted hydrotreating catalyst precursors. J Catal 132:498–511

[44] Song R, Luo B, Geng J, Song D (2018) Photothermocatalytic hydrogen evolution over Ni_2P/TiO_2 for full-spectrum solar energy conversion. Ind Eng Chem Res 57:7846–7854

[45] Gonçalves VOO, Brunet S, Richard F (2016) Hydrodeoxygenation of cresols over Mo/Al_2O_3 and $CoMo/Al_2O_3$ sulfided catalysts. Catal Lett 146:1562–1573

[46] Furimsky E (2000) Catalytic hydrodeoxygenation. Appl Catal A Gen 199:147–190

[47] Oyama S, Lee Y (2008) The active site of nickel phosphide catalysts for the hydrodesulfurization of 4,6-DMDBT. J Catal 258:393–400

[48] Lee Y-K, Seo H-R, Cho K-S, Kim S-H (2010) Effects of phosphorus precursor on structure and activity of Ni_2P/SiO_2 hydrotreating catalysts: EXAFS studies. J Korean Phys Soc 56:2083–2087